Thin Solid Films 638 (2017) 96–104

Contents lists available at ScienceDirect

Thin Solid Films

journal homepage: www.elsevier.com/locate/tsf

Nano mechanical and wear properties of multi-layer Ti/TiN coatings deposited on Al 7075 by high-vacuum magnetron sputtering

Sajjad Ghasemi [a], Ali Shanaghi [a,*], Paul K. Chu [b]

[a] Materials Engineering Department, Faculty of Engineering, Malayer University, Malayer, Iran
[b] Department of Physics and Department of Materials Science and Engineering, City University of Hong Kong, Tat Chee Avenue, Kowloon, Hong Kong, China

ARTICLE INFO

Article history:
Received 4 March 2017
Received in revised form 15 July 2017
Accepted 19 July 2017
Available online 20 July 2017

Keywords:
Multilayer coatings
Titanium
Titanium nitride
Magnetron sputtering
Mechanical properties
Wear
Lubrication

ABSTRACT

Super-hard coatings are frequently applied to improve the mechanical properties and abrasive properties of light alloys such as titanium and aluminum. In this work, single-layer TiN and multi-layer Ti/TiN coatings are deposited on Al 7075 by ultra-high vacuum magnetron sputtering and the structure, morphology, and triobological properties are investigated. The impact of the Ti layer on the microstructure, mechanical, and abrasive properties are also studied in details. The coatings containing the single TiN layer and Ti/TiN multi-layer crystal have the (111) and (002) preferred orientations. The hardness values of the single-layer and multi-layer coatings are 45.93 and 35.54, which are about 25 and 19 times larger than that of the substrate, respectively. The coefficients of friction of the multi-layer and single-layer coatings are 0.48 and 0.54, respectively. In the multi-layer coating, the Ti interlayer has smaller shear strength and acts as a lubricant during the abrasion test to reduce the friction. The $TiAlN_xO_y$ and TiN_xO_y tribolayers may be formed in the single-layer and multi-layer coatings, respectively and compared with the single-layer coatings, the multilayer ones have better tribological properties.

1. Introduction

7075 aluminum alloy is one of the important and widely used engineering alloys in aircrafts due to the large strength-to-density ratio and protective coatings are often applied to improve the surface properties such as hardness, friction, resistance to abrasion, and corrosion [1]. For instance, hard ceramic coatings are used to extend the life time and improve the load-bearing capacity of machines, tools, and biomedical implants. One of the common transition metal nitrides is titanium nitride (TiN) [2]. In practice, a multi-layer coating system allows a combination of high hardness, excellent wear resistance, corrosion resistance, and scratch resistance due to the combined merits of the ceramic layers and toughness of the metal layers [3]. Among super hard coatings such as TiAlN, TiAlCrN, TiCN, and TiN, TiN is easier to deposit but a soft surface may not be compatible with super hard coatings [2–4]. In this respect, multi-layer Ti/TiN coatings improve the corrosion and adhesion resistance as well as fatigue corrosion behavior of metal substrates while reducing the internal stress in coatings [5–7]. The softer Ti layer has a smaller shear strength serving as a solid lubricant during wear and so the coefficient of friction is reduced [3]. In multi-layer coatings, the role of the metal layers is stress reduction and increased resistance to failure. In comparison, in thin single-layer systems, cracks often develop on the surface and spread beneath the interface throughout the coatings. In coatings with a columnar microstructure, these cracks spread in the columnar boundaries and deformation proceeds by a sequence of ceramic layer breakage and metal yielding [8]. In this study, single-layer TiN and multi-layer Ti/TiN coatings are deposited on Al 7075 by high-vacuum magnetron sputtering and the structure, morphology, and mechanical properties are studied systematically. The Ti interlayer improves the adhesion strength and mechanical properties.

2. Materials and methods

The Al 7075 alloy was cut into circles with a radius of 1 cm and polished with sand paper from 800 to 4000 and then alumina paste with a diameter of 0.1 to 0.3 μm. The polished samples were rinsed ultrasonically in acetone, alcohol, and distilled water. The single-layer TiN and multi-layer Ti/TiN coatings were deposited by high-vacuum magnetron sputtering using a 99.99% pure Ti target. Before deposition, the samples were cleaned by energetic argon ion bombardment. In the deposition of the multi-layer coating, a titanium interlayer was first deposited and then TiN was deposited when nitrogen was bled into the vacuum chamber. The important deposition parameters are listed in Table 1.

The phase, structure, chemical composition, and morphology of the nanostructured coatings were examined by GIXRD (glancing incidence X-ray diffraction, Philips PW-1730 X-ray diffractometer, $CuK_\alpha\lambda$ = 0.154056 nm), XPS (X-ray photoelectron spectroscopy) and FE-SEM (field-emission scanning electron microscopy, JSM7001F)·The film

* Corresponding author.
E-mail addresses: a.shanaghi@malayeru.ac.ir, alishanaghi@gmail.com (A. Shanaghi).

http://dx.doi.org/10.1016/j.tsf.2017.07.049
0040-6090/

Table 1
Important deposition parameters.

Parameters		Time (min)	Power (watt)	Pressure (Pa)	Ar gas flow (sccm)	N_2 gas flow (sccm)
Multi-layer	Ti layer	15	220–280	0.43	14–17	–
	TiN sublayer	25	220–280	0.59	14–17	8–10
	TiN final layer	60	220–280	0.59	14–17	8–10
Single-layer	TiN	145	220–280	0.59	14–17	8–10

composition was determined by X-ray photoelectron spectroscopy (XPS, PHI 5802) using monochromatic Al K_α radiation. An argon ion beam was used to sputter about 20, 566, 770, and 910 nm of the surface in the depth profile analysis. The thickness of the coatings was determined by two methods, cross section examination and XPS depth profiling with sputtering rate of 20 nm/min. The nano mechanical properties such as Young's modulus (E) and hardness were determined by nanohardness tests conducted on the Hysitron TriboScope. The 142.38 Berkovich and cono-spherical radius ($R = 1.0$ mm) indenter supplied by SURFACE, Huck-elhoven was used. This test was done by the load control method [9] in which the load applied to the indenter was increased gradually until a predetermined maximum load and then reduced continuously to zero and the load and relevant diamond tip displacement were recorded. The hardness and elastic modulus were obtained from the continuous loading and unloading curves using Oliver-Phar method [10]. The indented surface made by the indenter with the Berkovich geometry depended on the contact depth calculated by Eq. (1) [11]:

$$A(h_c) = 24.56h_c^2 \tag{1}$$

where h_c is the depth of contact. The hardness was obtained by Eq. (2) and dividing the maximum applied load by the contact surface [11]:

$$\left(H = \frac{F_{max}}{A(h_c)}\right) \tag{2}$$

The elastic modulus [11] is defined based on the initial unloading contact hardness, S = dF/dh, *i.e.* slope of the initial part of the unloading curve as shown in Eq. (3):

$$\left(E_r = \frac{S}{2\beta}\sqrt{\frac{\pi}{A(h_c)}}\right) \tag{3}$$

where β is a constant that depends on the geometry of the indenter (β = 1.034 for Berkovich indentation) and E_r is the decreasing elastic modulus used for elastic deformation which occurs in both the sample and indenter. E is obtained from Eq. (4):

$$\left(\frac{1}{E_r} = \frac{(1-\nu^2)}{E} + \frac{1-\nu_i^2}{E_i}\right) \tag{4}$$

E and υare the elastic modulus and Poisson's ratio of the sample, respectively, Ei and υ_i are the similar amounts for the indenter, and E_r is the reduced elastic modulus. For diamond, $E_i = 1141$ GPa and $\upsilon_i = 0.07$ [10]. A pin-on-disk tribometer with a tungsten carbide pin ($5 * 10^{-3}$ m in diameter with roughness of 3×10^{-7} to 1×10^{-7} m) was used to determine the dry friction and wear performance of the coatings at 25 °C and 56% relative humidity. A constant load of 2 N and linear speed of 300 mm/min were used for a total length of 180,000 mm (500 cycles).

3. Results and discussion

Fig. 1 shows the patterns of the TiN and Ti/TiN coatings revealing the crystallographic directions. They can be indexed to the TiN phase standard cards (PFD # 38-1420), Al 7075 (PDF # 01-1176), and titanium (PDF # 01-1197). The TiN film shows the (111) preferred orientation. In the Ti/TiN coating, the film structure does not change but the intensity of the (111) peak decreases. The Ti layer shows the preferred orientation of (002) and growth of the TiN is along the same direction to reduce

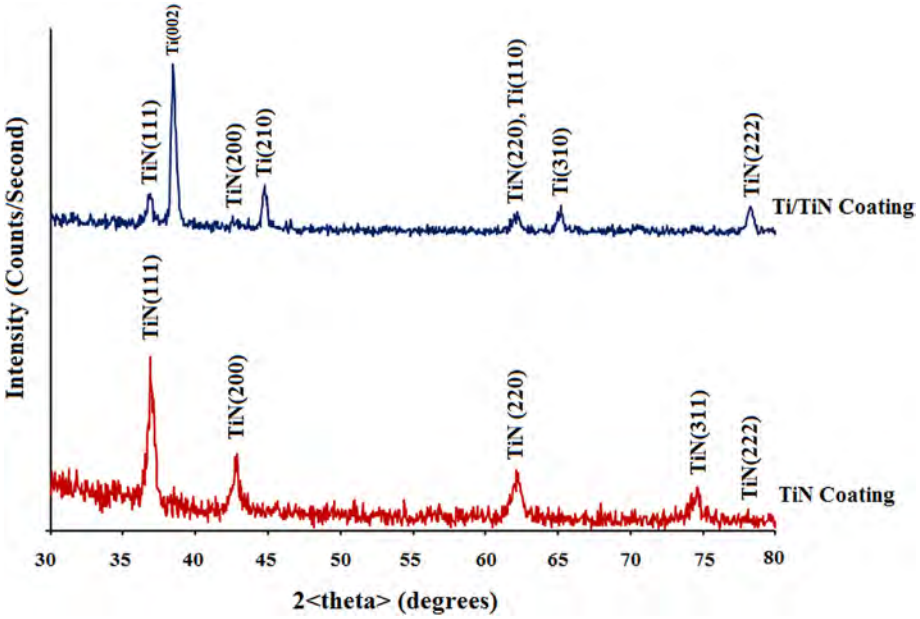

Fig. 1. GIXRD patterns of the TiN and Ti/TiN coatings.

Table 2
Thickness of Ti/TiN and TiN coatings.

Samples	Type of layer	Thickness of each layer (nm)	Total thickness (nm)
Single layer TiN coating	TiN	1350	1350
Multi-layer Ti/TiN coating	Ti(sub-layer)	150	1400
	TiN(sub-layer)	200	
	Ti(sub-layer)	150	
	TiN(sub-layer)	200	
	Ti (sub-layer)	150	
	TiN (top-layer)	550	

the interfacial energy [12]. In general, the Ti/TiN coating shows the preferred direction of Ti (002) and TiN (111) suggesting that most TiN plates (111) accumulate on Ti (002) [13]. The size of the TiN nanocrystallite can be estimated by Scherrer formula [14,15]:

$$L_{hkl} = \frac{k.\lambda}{\beta_{hkl}\cos\theta_{hkl}} \tag{5}$$

where β_hkl (FWHM) has the radian unit, θ_{hkl} is the Bragg angle, k is the Scherrer constant (equal to 0.9 for spherical beads), and λ is the wavelength of the X-ray (0.1541874 nm).The grain sizes of TiN and Ti are shown in Table 2 and similar results have been reported by Subramanian et al. [11]. The small crystallites produce a tough and hard surface [16]. The network parameters of TiN with the fcc structure and Ti are calculated by Eqs. (6) and (7) as follows:

$$\frac{1}{d^2} = \frac{h^2 + k^2 + l^2}{a^2} \tag{6}$$

and

$$\frac{1}{d^2} = \frac{4}{3}\left(\frac{h^2 + hk + k^2}{a^2}\right) + \frac{l^2}{c^2} \tag{7}$$

The obtained values are smaller than those determined from the bulk materials implying the existence of nitrogen vacancies [13].

The FE-SEM images are depicted in Fig. 2. Unlike coatings deposited by arc ion plating [17] having defects in the coatings leading to premature corrosion and those deposited by reactive magnetron sputtering [13] showing pebble-shaped particles, the coatings prepared by high-vacuum sputtering have a tough surface with fine grains. In fact, the particles are fused and round being characteristic of the AIP method [18, 19]. Fig. 2d shows that the TiN coating has a common columnar structure in which the grain boundaries grow perpendicular to the substrate surface. This microstructure is compatible with the T region in the structural model of Thornton which is integrated with the region I in high ion bombardment [20]. In the multi-layer coatings, as the ratio of the thickness of Ti/TiN is increased (proportional to the accumulation time ratio of Ti/TiN), the layer becomes micro-structural (Fig. 2b).The Ti/TiN columnar growth is intersected by the Ti interlayer [21]. The thickness of the coatings is summarized in Table. 2.

Fig. 3 shows the curves of the load and displacement for aluminum 7075, TiN, and Ti/TiN. The two mechanical parameters which are frequently determined by indentation are hardness (H) and elastic modulus (E). The curve exhibits two elastic and plastic deformation parts and by removing the load, only the elastic part of the displacement is retrieved. The use of elastic solutions in modeling facilitates the contact process [21]. According to Fig. 3, TiN, Ti/TiN, and Al are subjected to loads of 459, 343.3 and 157.7 mN, respectively, and indentation depths of 10 to 15% of the coating thickness.

As shown in Fig. 3 and Table 2, the hardness of both coatings is larger than that of the substrate. As shown in Fig. 4a, changes in the slope of the TiN sample and downward displacements mainly reflect the

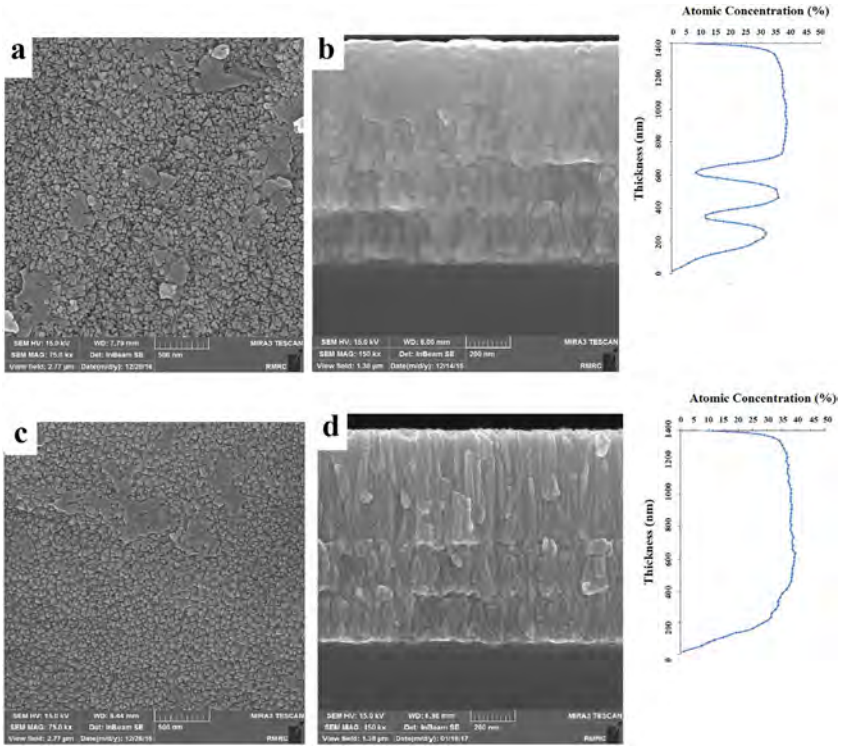

Fig. 2. FE-SEM images and XPS depth profile of N1s: (a, b) Multi-layer Ti/TiN and (c, d) Single-layer TiN.

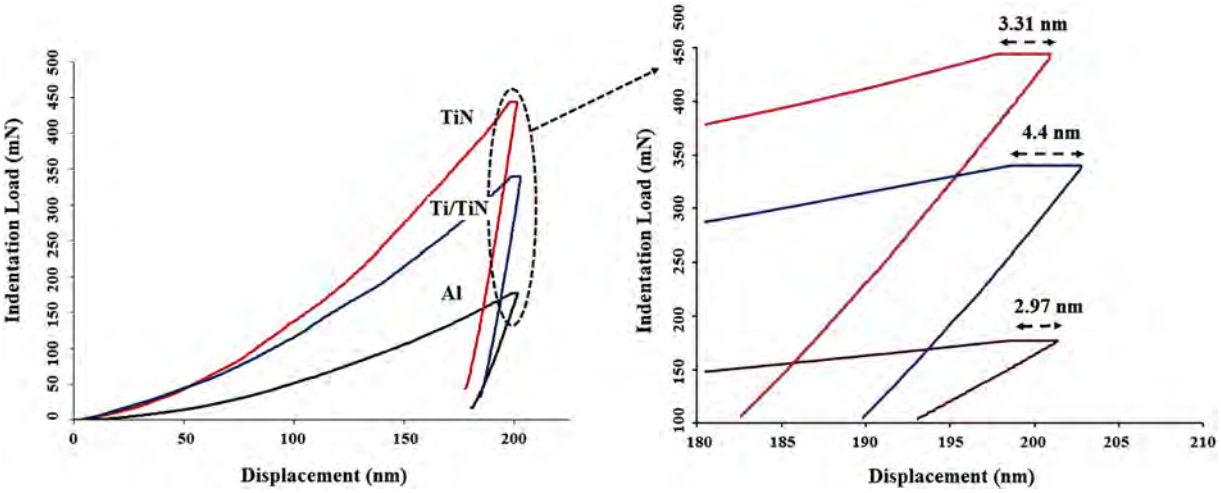

Fig. 3. Load – displacement curves of the multi-layer Ti/TiN, single-layer TiN, and Al 7075 substrate.

elastic-to-plastic deformation and some pop-ins are observed from the graphs possibly due to cracking in the coatings [22]. The H^3/E^2values of TiN and Ti/TiN are shown in Table 3. The resistance to plastic deformation (H^3/E^2) shows strong resistance to plastic deformation in the elastic-to-plastic contact plates [23].

Owing to the presence of TiN as a super hard layer, the multi-layer coating is harder than the substrate [20]. However, with increasing thickness ratio of Ti/TiN, the hardness of the multi-layer coatings diminishes gradually. Similar results have been obtained by Cheng et al. [3]. With respect to Ti/TiN and Al 7075, the region of elastic-to-plastic deformation is not observed (Fig. 3) because of the small area. The hardness values of the single-layer and multi-layer coatings are, respectively, 45.93 and 35.54 GPa and the single-layer coating is harder. At large indentation depths, the hardness and elastic modulus measured from the Ti interlayer decrease. According to the rule of mixture [24], increasing the volume mass of the softer Ti interlayer which is more prone to plastic deformation reduces the hardness. As a result, when the diamond tip penetrates more deeply in the Ti/TiN multi-layer coatings, lower hardness and modulus are observed [25]. Increasing the number of layers in multi-layer actually decreases the porosity and grain size. According to the Hall-Petch effect, a large refinement grain size leads to locked dislocation or restriction and reduces the surface tension. All these parameters increase the quality and hardness of the coating as well as resistance to corrosion. A smaller crystallite size improves the surface morphology and microstructure by reducing the roughness [26].

The plasticity can be determined by nano-hardness tests. During loading, if the unloading-displacement curves do not overlap, plasticity can be determined by the ratio of residual displacement to the total displacement [25,27–28].

$$Plasticity = \frac{\varepsilon_p}{\varepsilon} = \frac{D_r}{D_{max}} \tag{8}$$

The plasticity values of the single-layer and multi-layer coatings are 86.4 and 91.1, respectively, with that of the multi-layer coating being larger. An increase of 5% is observed after introducing the TiN interlayer. The larger plasticity is attributed to the Ti component and the high plasticity of the single-layer coating (86.4) is quite large on account of the columnar structure.

In addition to the hardness, elastic modulus, and elastic-plastic behavior of the coatings, the nano-indentation curves reveal the creep behavior [29] according to the change in the depth of indentation under a constant load. In the nano-indentation test, creep and plastic deformation occur interchangeably. Since creep is gradual deformation of the

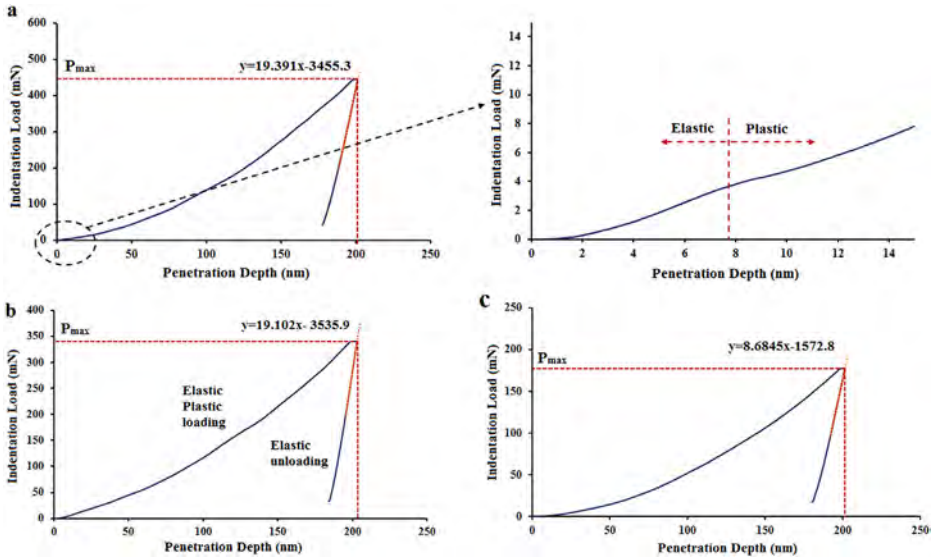

Fig. 4. Calculation of elastic to plastic deformation, contact stiffness, and maximum load in the samples: (a) TiN, contact stiffness and maximum loads in sample (b) Ti/TiN and (c) Al 7075.

Table 3
Parameters obtained from the load-displacement curves of Al 7075, single-layer TiN, and multi-layer Ti/TiN coatings.

Sample	H (GPa)	E (GPa)	H^3/E^2 (GPa)	P (%)	S	μ
Al 7075	1.85	75.66	0.00106	88.3	8.68	0.51
TiN	45.93	168.95	3.38	86.4	19.39	0.54
Ti/TiN	35.54	166.43	1.62	91.1	19.1	0.48

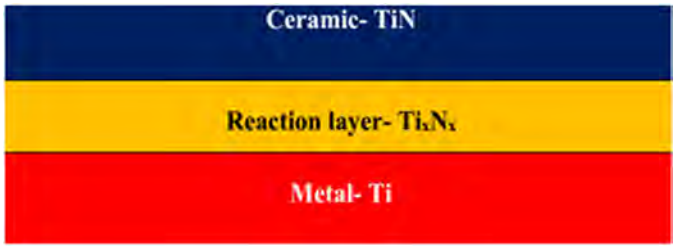

Fig. 5. Schematic of the reaction layer in the Ti/TiN multi-layer coating.

coating or sample, it must be examined separately. In fact, plasticity indicates the yield or hardness in a momentary event, although in practice, it can be referred to as the yield time. According to Fig. 4 (the dotted part), the creep level of Ti/TiN is higher than that of TiN due to the Ti interlayer may be that facilitating grain boundary sliding, grain rotation, and dislocation climb in multi-layer Ti/TiN coating and increasing the creep level. Generally, creep in plastic deformation can be the result of movement of atoms or movement of dislocations in the tension field of indentation or through the activation of shear transformation mechanisms, and is highly dependent on the temperature [30–31]. If the effects caused by deformation of cracks are ignored, permanent deformation under indentation loading is a combination of immediate plasticity (time-independent) and creep (time-dependent). The term "creep" is often used for a delayed response to the stress or strain which may be the result of a viscoelastic or viscoplastic deformation.

Creep can be caused by the chemical potential gradient proportional to the concentration of stress which activates the influx by heat. As a result, the atoms flow from the area under the indenter to the sample surface along the interface between the indenter and sample even under an elastic contact [29–32]. The creep lengths for Ti/TiN and TiN are, respectively, 4.4 nm and 3.31 nm. In multilayered coatings, a Ti intermediate layer (Fig. 5) can be increased grain boundary more than that of TiN and increases the creep in the multi-layer coatings. Verification of this phenomenon requires further investigation and analysis such as TEM.

Fig. 6 shows the changes in the coefficients of friction revealing two steps: the first step with high friction and a fixed stage showing friction reduction. In the first step, the coefficients of friction depend on the film roughness and a conductive layer (tribolayer) is created. In the second step, friction and wear depend on the nature of the tribolayer [33].

The small coefficient of friction in the early wear stages of multilayer Ti/TiN coatings compared to those of the uncoated substrate and single-layer coating can be attributed to the roughness. In fact, with increasing roughness, the roughness of the surface increases leading to increased engagement of abrasive particles and more parts of the coating surface consequently increasing the coefficient of friction [34]. The TiN coatings have higher resistance to abrasion. There is a large expansion coefficient difference between the aluminum substrate and TiN coating thus leading to higher thermal stress during the process. In the presence of the Ti interlayer, the thermal expansion coefficient difference decreases and as a result, the adhesion strength between the film and substrate increases [23]. In general, by increasing the surface hardness, the

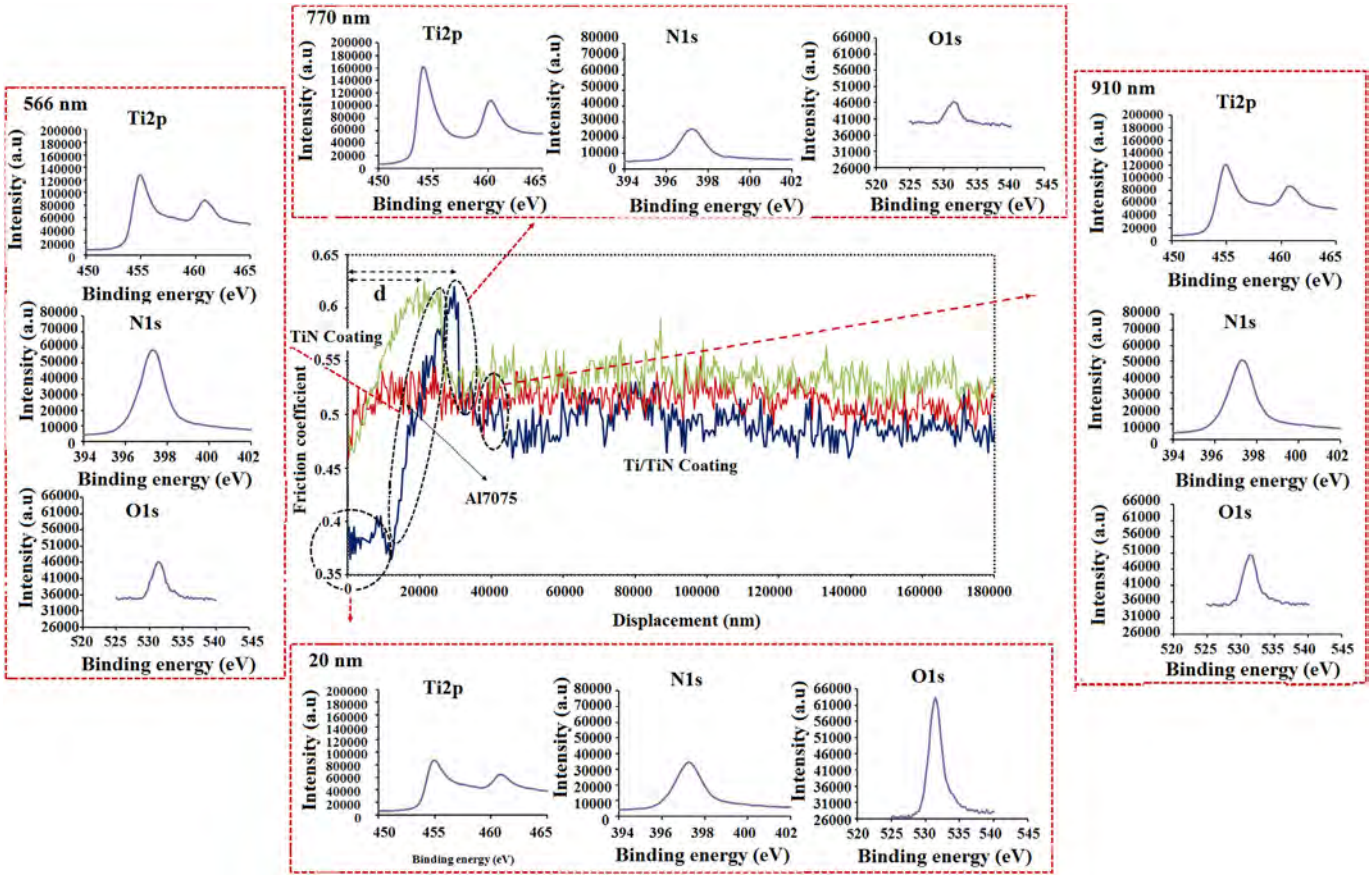

Fig. 6. Curves of friction coefficients of the coatings and Al 7075 substrate.

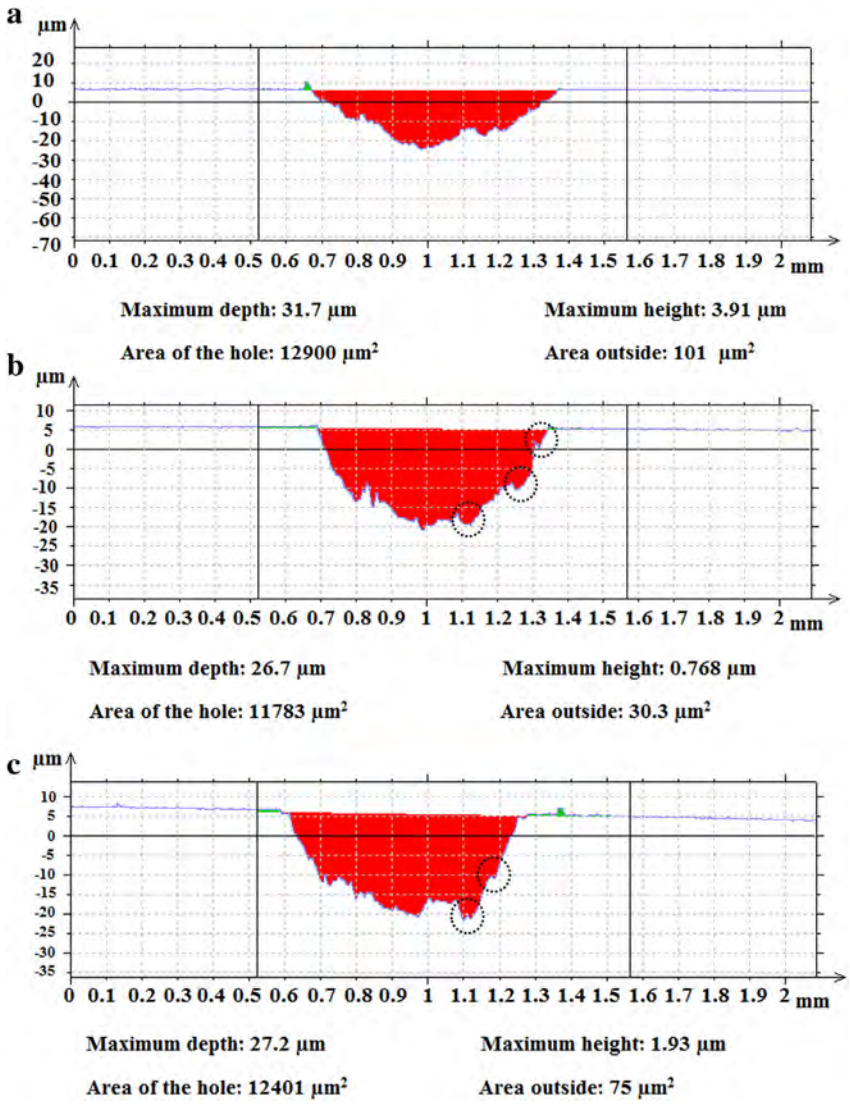

Fig. 7. Cross-sectional profiles of the wear path on (a) Al 7075, (b) TiN, and (c) Ti/TiN.

coating attrition rate is reduced [35]. According to Fig. 6, the Ti/TiN coating has a smaller coefficient of friction than the TiN coating and aluminum 7075. The coefficient of friction of the TiN coating is 0.54 and after introduction of the Ti interlayer, it drops to 0.48 which is similar to values previously reported [25]. The slight decrease in the friction coefficient in the steady state with the Ti layer in the film arises from the reduced roughness which increases the contact surface. The Ti and TiN layers have different crystal structures and there is lattice mismatch between the borders of the Ti and TiN layers creating a tension area in both layers and hindering movement of dislocations in the Ti layer. In the Ti/TiN coating, the tension field in both layers is distributed mainly in the Ti layer and larger stress is required for plastic deformation in the Ti layer. Consequently, a larger sliding gap is required for the sudden decrease in the coefficient of friction (distance d in Fig. 6) [25]. Owing to the multilayered structure, the abrasion process produces a transition between the hard layer of TiN and soft layer of Ti. When the abrasive pin wears the Ti soft layer, lubrication is carried out and the coefficient of friction is reduced during the movement of the multi-layer interface. The coefficient of friction swings upward and downward in the hard and soft layers, respectively. Hence, the wear mechanism between the WC pin and Ti/TiN coating is mainly that of scratching [34]. The soft Ti layer has smaller shear strength and acts as a solid lubricant during wear [25]. This is manifested as reduced coefficients of friction for Ti/TiN as shown in Fig. 6. XPS reveals the wear mechanism of the multi-layer Ti/TiN coatings for different thicknesses. As shown in Fig. 6 (bottom), oxidation is observed at a thickness of 20 nm reducing the coefficient of friction. At a thickness of 566 nm (left), the percentages of titanium and nitrogen increase due to the TiN layer and the coefficient of friction increases. At a thickness of 770 nm (Fig. 6 (up)), the nitrogen percentage decreases due to the Ti layer which has smaller shear strength and reduces the coefficient of friction. At a thickness of 910 nm, the amounts of titanium and nitrogen increase again due to abrasive pin penetration into the next TiN layer thereby increasing the coefficient of friction (Fig. 6 (right)).

The cross-sectional profiles of the wear tracks in Fig. 7 disclose some cavities and grooves. There are grooves (dotted circles in Fig. 7) in the direction of the coating path of TiN and Ti/TiN reaching the Ti/TiN substrate surface resulting in fluctuations in the coefficients of friction. With regard to the TiN coating (Fig. 7b), these grooves from a smaller area than the substrate. After introduction of the Ti interlayer, the

Table 4
Parameters obtained from the cross-sectional profiles of the wear tracks.

Samples	h(μm)	h_c(μm)	h_c/h
Al	31.7	35.61	1.12
TiN	26.7	27.46	1.02
Ti/TiN	27.2	29.13	1.07

number of grooves decreases representing reduction in friction and scratch wear [36]. As shown in Fig. 7, there is almost no difference in the contact widths on the samples. The depth of scratch is measured below the primary level h and overall depth h_c and summarized in Table 4. h_c/h represents piling up of the coating [37] reflecting less plastic deformation. After the test, the profiles generally show a regular shape with very little pile-ups on the edges of the scratch track indicating abrasive wear [38].

To study the wear mechanism, the wear tracks are examined by FE-SEM as shown in Fig. 8. On the TiN coating, the scratch track is shallow and soft reflecting excellent wear resistance of TiN [23]. Owing to the presence of heavy elements such as Ti in the BSE images, the scratch track is shown as white (brighter). In the single-layer TiN coating, arc cracks are observed on a large scale along the movement of the scraping tip indicative of sticky failure [36] and fragile coating. These cracks are caused by the lack of toughness of this layer and high hardness. On the multi-layer Ti/TiN coating, the scratch track is wider and rougher. Abrasive grooves are observed along the scratch track and there is no crack at the scratch edges (Fig. 8a) caused by plastic deformation of the Ti interlayer [39]. The cracks confirm the impact of the multi-layer coating at all the interfaces (cracks due to division or deviation) and deformation of the Ti soft substrate [40]. In the multi-layer coating,

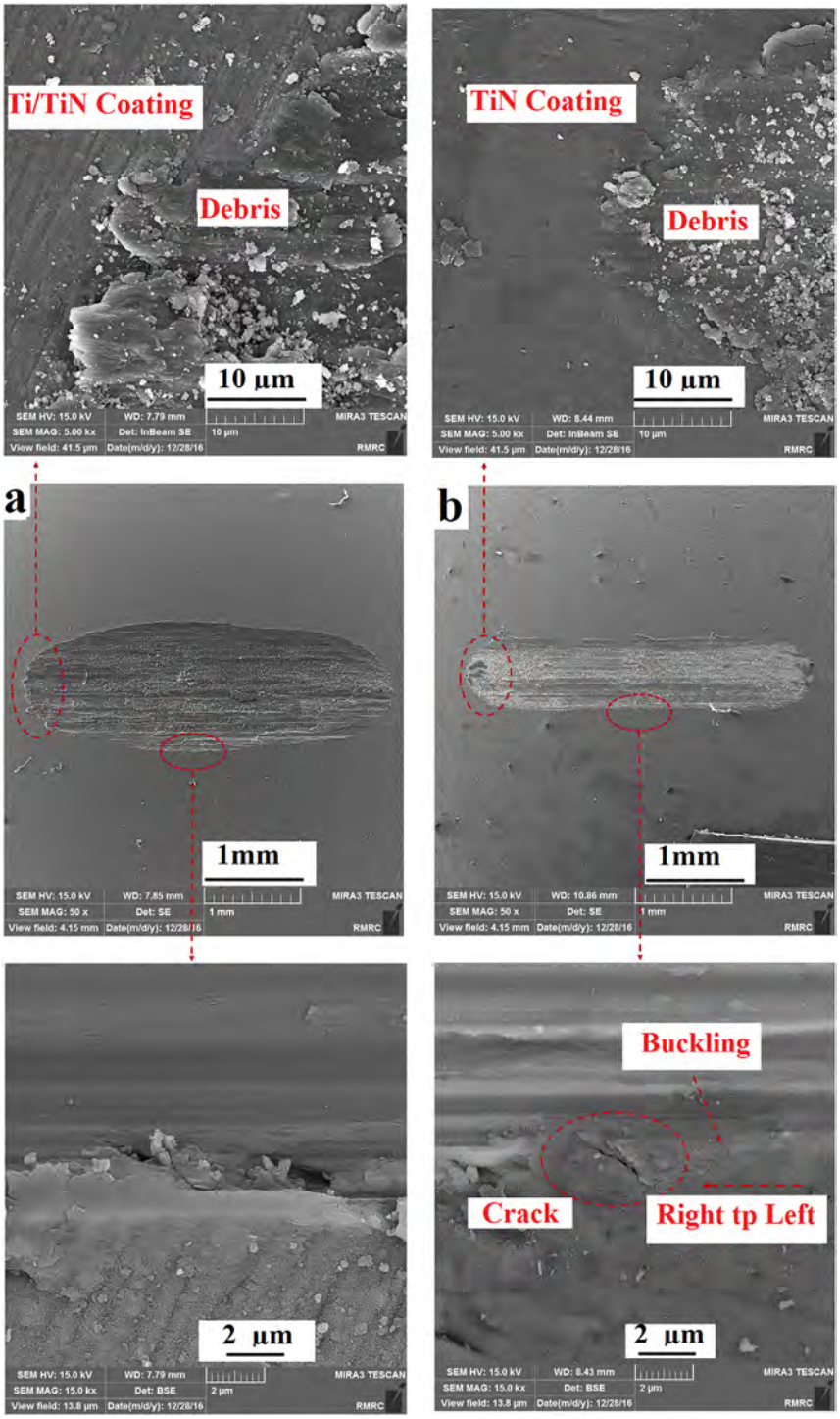

Fig. 8. FE-SEM images of the wear tracks: (a) Multi-layer Ti/TiN and (b) TiN.

deformation appears first with slip between the grains and Ti soft layer plastic flow [39] ultimately leading to high scratch resistance. This is because the films can enhance energy absorption without ductile breakage in the Ti layers. A larger load accentuates the impact of ploughing due to compressive stress in front of the pin [39,41]. As a result, irregular micro-cracks are spread by the pin developing bending and shear stress. Delamination of the TiN coating thus occurs at small loads while the multi-layer coating is more resistant against delamination. Cohesive failure can occur at the Ti/TiN interface [39] but severe delamination is not observed but severe plastic deformation is observed from the edges.

On the left and right sides of the contact area in Fig. 9, a tribofilm (transitional layer) containing Ti, N, and O is formed. The pulverized materials are oxidized and accumulate on the borders. The tribolayers are formed during abrasion of both the TiN and Ti/TiN coatings as well as aluminum 7075 due to delamination and groove formation [39] and oxidation reduces the friction by forming a mixture with low ductility [42]. According to the EDS map taken from the scratch areas of the Ti/TiN coating in Fig. 9a and the TiN layer in Fig. 9b, Ti/TiN shows a higher degree of oxidation. Aluminum in incorporated as $TiAlN_xO_y$ in the tribolayer of the TiN single-layer coating. The TiN_xO_y tribolayer may be formed in the multi-layer coating. $TiAlN_xO_y$ is harder than TiN_xO_y [43] due to partial replacement of Al in TiN. The atomic radius difference between Al and Ti results in the solution strength leading to distortion of the network [34]. Formation of metal oxide in tribosystems with hard ceramic coatings, especially at small loads and sliding speeds, has been observed previously [8].

4. Conclusion

Ti/TiN and TiN coatings are deposited on aluminum by high-vacuum magnetron sputtering and the impact of the Ti interlayer on the nano mechanical and abrasive properties are studied. GIXRD shows the preferred (111) orientation in the TiN coating and it changes to (002) after introduction of the Ti interlayer. The coatings show excellent and adhesion with the substrate. The hardness values of the single-layer and multi-layer coatings are 45.93 and 35.54 GPa which are about 25 and 19 times larger than that of the substrate, respectively. The coefficients of friction of the multi-layer and single-layer coatings are 0.48 and 0.54, respectively. According to the elemental maps, the $TiAlN_xO_y$ and TiN_xO_y tribolayers are observed from the single- and multi-layer coatings.

Acknowledgements

The authors would like to thank the Iranian Nanotechnology Initiative Council. The work was financially supported by Malayer University

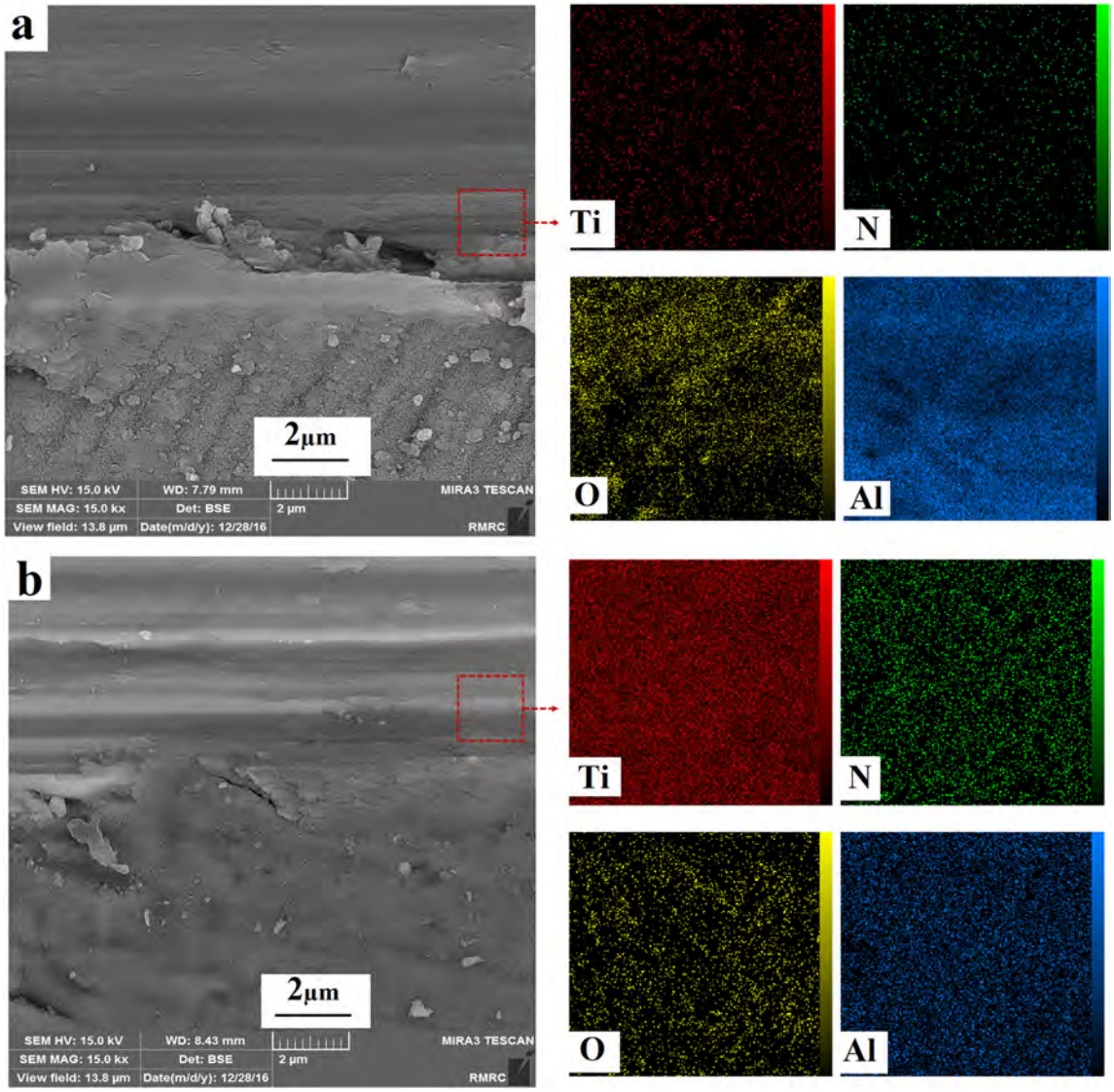

Fig. 9. Elemental maps in the scratch areas on the coatings: (a) Multi-layer Ti/TiN and (b) Single-layer TiN.

Research Grant and Iran National Science Foundation, Hong Kong Research Grants Council (RGC) General Research Funds (GRF) No. CityU 11301215, and City University of Hong Kong Applied Research Grant No. 9667122.

References

[1] R. Oskouei, R. Ibrahim, An investigation on the fatigue behaviour of Al 7075-T6 coated with titanium nitride using physical vapour deposition process, Mater. Des. 39 (2012) 294–302.
[2] W. Feng, D. Yan, J. He, X. Li, Y. Dong, Reactive plasma sprayed TiN coating and its tribological properties, Wear 258 (5–6) (2005) 806–811.
[3] Y.H. Cheng, T. Browne, B. Heckerman, C. Bowman, V. Gorokhovsky, E.I. Meletis, Mechanical and tribological properties of TiN/Ti multilayer coating, Surf. Coat. Technol. 205 (1) (2010) 146–151.
[4] D. Dinesh Kumar, N. Kumar, S. Kalaiselvam, S. Dash, R. Jayavel, Wear resistant superhard multilayer transition metal-nitride coatings, Surf. Interfaces 7 (2017) 74–82.
[5] Y. Cheng, T. Browne, B. Heckerman, J. Jiang, E. Meletis, C. Bowman, V. Gorokhovsky, Internal stresses in TiN/Ti multilayer coatings deposited by large area filtered arc deposition, J. Appl. Phys. 104 (9) (2008), 093502. http://dx.doi.org/10.1063/1.3006136.
[6] R. Hübler, A. Schröer, W. Ensinger, G. Wolf, F. Stedile, W. Schreiner, I. Baumvol, Corrosion behavior of steel coated with thin film TiN/Ti composites, J. Vac. Sci. Technol. A 11 (2) (1993) 451–453.
[7] X. Zhang, D. Liu, H. Tan, X. Wang, Effect of TiN/Ti composite coating and shot peening on fretting fatigue behavior of TC17 alloy at 350 °C, Surf. Coat. Technol. 203 (16) (2009) 2315–2321.
[8] M. Kot, Contact mechanics of coating-substrate systems: monolayer and multilayer coatings, Arch. Civ. Mech. Eng. 12 (4) (2012) 464–470.
[9] T.S. Li, H. Li, F. Pan, Microstructure and nanoindentation hardness of Ti/TiN multilayered films, Surf. Coat. Technol. 137 (2–3) (2001) 225–229.
[10] W.C. Oliver, G.M. Pharr, An improved technique for determining hardness and elastic modulus using load and displacement sensing indentation experiments, J. Mater. Res. 7 (06) (1992) 1564–1583.
[11] X. Li, B. Bhushan, A review of nanoindentation continuous stiffness measurement technique and its applications, Mater. Charact. 48 (1) (2002) 11–36.
[12] G. Kim, S. Lee, J. Hahn, B. Lee, J. Han, J. Lee, Effects of the thickness of Ti buffer layer on the mechanical properties of TiN coatings, Surf. Coat. Technol. 171 (1) (2003) 83–90.
[13] B. Subramanian, R. Ananthakumar, M. Jayachandran, Structural and tribological properties of DC reactive magnetron sputtered titanium/titanium nitride (Ti/TiN) multilayered coatings, Surf. Coat. Technol. 205 (11) (2011) 3485–3492.
[14] S. Logothetidis, P. Patsalas, C. Charitidis, Enhanced catalytic activity of nanostructured cerium oxide films, Mater. Sci. Eng. C 23 (6–8) (2003) 803–806.
[15] R. Yogamalar, R. Srinivasan, A. Vinu, K. Ariga, A.C. Bose, X-ray peak broadening analysis in ZnO nanoparticles, Solid State Commun. 149 (43–44) (2009) 1919–1923.
[16] Y.-H. Chen, K.W. Lee, W.-A. Chiou, Y.-W. Chung, L.M. Keer, Synthesis and structure of smooth, superhard TiN/SiNx multilayer coatings with an equiaxed microstructure, Surf. Coat. Technol. 146–147 (2001) 209–214.
[17] P.J. Martin, A. Bendavid, Review of the filtered vacuum arc process and materials deposition, Thin Solid Films 394 (1–2) (2001) 1–14.
[18] L. Chenglong, Y. Dazhi, L. Guoqiang, Q. Min, Corrosion resistance and hemocompatibility of multilayered Ti/TiN-coated surgical AISI 316L stainless steel, Mater. Lett. 59 (29) (2005) 3813–3819.
[19] J. Bolton, X. Hu, In vitro corrosion testing of PVD coatings applied to a surgical grade Co–Cr–Mo alloy, J. Mater. Sci. Mater. Med. 13 (6) (2002) 567–574.
[20] J.A. Thornton, High rate thick film growth, Annu. Rev. Mater. Sci. 7 (1) (1977) 239–260.
[21] D. Zhou, H. Peng, L. Zhu, H. Guo, S. Gong, Microstructure, hardness and corrosion behaviour of Ti/TiN multilayer coatings produced by plasma activated EB-PVD, Surf. Coat. Technol. 258 (2014) 102–107.
[22] L. Ma, J. Cairney, M. Hoffman, P. Munroe, Characterization of TiN thin films subjected to nanoindentation using focused ion beam milling, Appl. Surf. Sci. 237 (1) (2004) 627–631.
[23] X. Liu, G.J. Ma, G. Sun, Y.P. Duan, S.H. Liu, The influence of Ti doping on the mechanical properties of TaN film, Surf. Coat. Technol. 212 (2012) 128–133.
[24] A.E. Santana, A. Karimi, V.H. Derflinger, A. Schütze, Microstructure and mechanical behavior of TiAlCrN multilayer thin films, Surf. Coat. Technol. 177–178 (2004) 334–340.
[25] Y. Cheng, T. Browne, B. Heckerman, C. Bowman, V. Gorokhovsky, E. Meletis, Mechanical and tribological properties of TiN/Ti multilayer coating, Surf. Coat. Technol. 205 (1) (2010) 146–151.
[26] S. Wulfinghoff, E. Bayerschen, T.s Böhlke, Micromechanical simulation of the Hall-Petch effect with a crystal gradient theory including a grain boundary yield criterion, Minisymposia Mech. 2 (13) (2013) 15–18.
[27] Y.V. Milman, B. Galanov, S. Chugunova, Plasticity characteristic obtained through hardness measurement, Acta Metall. Mater. 41 (9) (1993) 2523–2532.
[28] S. Zhang, D. Sun, Y. Fu, H. Du, Toughness measurement of thin films: a critical review, Surf. Coat. Technol. 198 (1) (2005) 74–84.
[29] A.C. Fischer-Cripps, Nanoindentation testing, Nanoindentation, Springer 2011, pp. 21–37.
[30] X. Wang, P. Gong, L. Deng, J. Jin, S. Wang, P. Zhou, Nanoindentation study on the room temperature creep characteristics of a senary $Ti_{16.7}Zr_{16.7}Hf_{16.7}Cu_{16.7}Ni_{16.7}Be1_{6.7}$ high entropy bulk metallic glass, J. Non-Cryst. Solids 470 (2017) 27–37.
[31] C. Wang, Q.P. Cao, X.D. Wang, D.X. Zhang, S.X. Qu, J.Z. Jiang, Time-dependent shear transformation zone in thin film metallic glasses revealed by nanoindentation creep, J. Alloys Compd. 696 (2017) 239–245.
[32] W. Li, R. Warren, A model for nano-indentation creep, Acta Metall. Mater. 41 (10) (1993) 3065–3069.
[33] D. Liu, J. Tu, C. Hong, C. Gu, Y. Mai, R. Chen, Improving mechanical properties of a-CN × films by Ti–TiN/CN × gradient multilayer, Appl. Surf. Sci. 257 (2) (2010) 487–494.
[34] W. Yongqiang, Z. Xiaoya, W. Zhongzhen, T. Xiubo, G. Chunzhi, Y. Shiqin, J. Zhiqiang, C. Liangji, Effects of modulation ratio on microstructure and properties of TiN/TiAlN multilayer coatings, Surf. Coat. Technol. 229 (2013) 191–196.
[35] J. Yue, Y. Liu, G. Li, Template-induced coherent growth and mechanical properties of ZrO 2/TiN nano-multilayers, Scr. Mater. 60 (4) (2009) 240–243.
[36] B. Tian, W. Yue, Z. Fu, Y. Gu, C. Wang, J. Liu, Microstructure and tribological properties of W-implanted PVD TiN coatings on 316L stainless steel, Vacuum 99 (2014) 68–75.
[37] Y. Xie, H.M. Hawthorne, Effect of contact geometry on the failure modes of thin coatings in the scratch adhesion test, Surf. Coat. Technol. 155 (2–3) (2002) 121–129.
[38] M. Kot, W. Rakowski, Ł. Major, J. Lackner, Load-bearing capacityof coating–substrate systems obtained from spherical indentation tests, Mater. Des. 46 (2013) 751–757.
[39] J. Lackner, L. Major, M. Kot, Microscale interpretation of tribological phenomena in Ti/TiN soft-hard multilayer coatings on soft austenitesteel substrates, Bull. Pol. Acad. Sci. Tech. Sci. 59 (3) (2011) 343–355.
[40] J.K. Park, C. Ziebert, M. Stüber, Y.J. Baik, Improvement of hardness and toughness of TiAlN coating by nanoscale multilayered structurization withSi3N4, Plasma Process. Polym. 4 (S1) (2007) S902–S905.
[41] A. Karimi, Y. Wang, T. Cselle, M. Morstein, Fracture mechanisms in nanoscale layered hard thin films, Thin Solid Films 420 (2002) 275–280.
[42] I.M. Hutchings, P. Shipway, Tribology: Friction and Wear of Engineering Materials, 1992.
[43] Y. Chim, X. Ding, X. Zeng, S. Zhang, Oxidation resistance of TiN, CrN, TiAlN and CrAlN coatings deposited by lateral rotating cathode arc, Thin Solid Films 517 (17) (2009) 4845–4849.